Inorganic Chemistry

Article

pubs.acs.org/IC

Theoretical Studies on the Photoelectron and Absorption Spectra of MnO_4^- and TcO_4^-

Jing Su,[†,‡] Wen-Hua Xu,[†] Chao-Fei Xu,[†] W. H. E. Schwarz,[†,§] and Jun Li*[,†]

[†]Department of Chemistry and Key Laboratory of Organic Optoelectronics and Molecular Engineering of the Ministry of Education, Tsinghua University, Beijing 100084, China

[‡]Shanghai Institute of Applied Physics, Chinese Academy of Sciences, Shanghai 201800, China

Supporting Information

ABSTRACT: The tetraoxo pertechnetate anion (TcO_4^-) is of great interest for nuclear waste management and radiopharmceuticals. To elucidate its electronic structure and to compare with that of its lighter congener MnO_4^-, the photoelectron and electronic absorption spectra of MnO_4^- and TcO_4^- are investigated with density functional theory (DFT) and *ab initio* wave function theory (WFT). The vertical electron detachment energies (VDEs) of MnO_4^- obtained with the CR-EOM-CCSD(T) method are in good agreement with the lowest two experimental VDEs; the differences are less than 0.1 eV, representing a significant improvement over the IP-EOM-CCSD(T) result in the literature. Combining our CCSD(T) and CR-EOM-CCSD(T) results, the first five VDEs of TcO_4^- are estimated between 5 and 10 eV with an estimated accuracy of about ±0.2 eV. The vertical excitation energies are determined by using TD-DFT, CR-EOM-CCSD(T), and RAS-PT2 methods. The excitation energies and the assignments of the spectra are analyzed and partly improved. They are compared with reported SAC-CI results and available experimental data. Both dynamic and nondynamic electron correlations are important in the ground and excited states of MnO_4^- and TcO_4^-. Nondynamical correlations are particularly relevant in TcO_4^- for reliable prediction of excitation energies. In TcO_4^- one Rydberg state interlaces but does not mix with the valence excited states, and it disappears in the condensed phase.

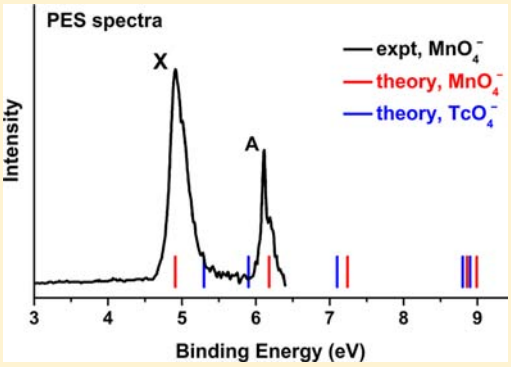

1. INTRODUCTION

Being the first predominantly synthetic element, technetium has a long-lived soft β-emitting ^{99}Tc isotope ($t_{1/2} = 2 \times 10^5$ years), which is available in high radionuclide purity from ^{99}Mo after β^- decay or by uranium fission in high yield (ca. 6%) in nuclear reactors. ^{99}Tc has many applications in the area of nuclear medicine and biology. A common form of Tc in water is the tetraoxo pertechnetate anion, and γ-radiating $^{99m}TcO_4^-$ is the most important radiopharmaceutical diagnostic.[1−3] In nuclear waste cleanup and nuclear fuel reprocessing such as the PUREX process, separating technetium (as TcO_4^-) in acidic solution from the major actinides is one of the major issues.[4,5]

Pertechnatate, a strong oxidizing reagent, belongs to the family of d^0 tetraoxo transition metal complexes, such as VO_4^{3-}, CrO_4^{2-}, MnO_4^-, RuO_4, and their heavier homologues. Their electronic structures have been the subject of numerous studies over the past 70 years. Experimentally, UV−vis absorption spectroscopy has become a common tool to study the electronic structure of inorganic transition metal compounds, and the electronic absorption spectra of TcO_4^- in vapor and solid phase were already reported in the 1970s.[6,7]

However, only a few theoretical studies were carried out on this molecule, most of which were based on DFT and TD-(time-dependent) DFT.[8−10] So far only one theoretical study was carried out at the post Hartree−Fock level using symmetry adapted cluster-configuration interaction (SAC-CI),[11] and there is our recent work[12] about Tc−O bond length change upon electronic excitation. Despite the importance of electronic spectroscopy in characterizing the electronic structures of TcO_4^-, no accurate theoretical studies of the excited electronic states and absorption spectra based on advanced *ab initio* methods have been reported yet. Anionic photoelectron (photodetachment) spectroscopy can also provide rich information on chemical bonding in the anion and on the ground and excited states of the neutral molecule, but there is no such experimental work on TcO_4^- so far. Concerning its lighter congener MnO_4^-, the classical permanganate, electronic spectra were measured and discussed already in the late 1930s[13,14] and 1960s.[6,15] Previous computational work on MnO_4^- has applied HF (Hartree−Fock),[16−18] post-HF,[19−23] and DFT[8,24−28] methods.

Therefore, we have theoretically investigated the electronic absorption and photoelectron spectra of TcO_4^- by calculating the vertical detachment energies (VDEs) and vertical excitation energies. The advanced *ab inito* WFT methods CR-EOM-CCSD(T) and RAS-PT2 were employed (CR = completely

Received: April 18, 2013
Published: August 19, 2013

 © 2013 American Chemical Society dx.doi.org/10.1021/ic4009625 | Inorg. Chem. 2013, 52, 9867−9874

renormalized; EOM = equation of motion; CC = coupled cluster; SD(T) = single, double, and perturbative triple substitutions; RAS = self-consistent restricted active space; PT2 = second order perturbation theory). These approaches had been used successfully for the accurate account of the electronic spectra of transition metal compounds[29] and actinide compounds[30−32] and compared with TDDFT. We also compare TcO_4^- with its lighter congener MnO_4^-. DFT and *ab initio* wave function approaches were applied to determine the photoelectron and absorption spectra of MO_4^- molecules (M = Mn, Tc), using the DFT, TDDFT, CCSD(T), CR-EOM-CCSD(T), and RAS-PT2 methods, respectively. The computational details of the applied methods are given in section 2. The results of the spectra are presented and discussed in section 3. Our main conclusions are drawn in section 4.

2. COMPUTATIONAL DETAILS

DFT and TD-DFT Approximations. For the ionization potentials, the neutral molecules MO_4 and anions MO_4^- (M = Mn, Tc) were first separately calculated at the DFT level. As exchange-correlation potential, the generalized gradient approximation (GGA) with the PBE functional[33] as implemented in the Amsterdam Density Functional program ADF2010.02 was chosen.[34−36] The frozen core approximation was applied to the inner atomic core shells: for Mn a Ne[$1s^2$−$2p^6$] core with 10 electrons, for Tc a [$1s^2$−$3d^{10}$] core with 28 electrons, and for O a He[$1s^2$] core with 2 electrons. The scalar relativistic (SR) and spin−orbit (SO) coupling effects were taken into account at the zero order regular approximation (ZORA).[37] Slater basis sets of triple-ζ double-polarization quality (TZ2P) as implemented in the program were used.[38] The geometries were fully optimized at the SR-ZORA level, and single-point energy calculations were performed with inclusion of the SO coupling effects via the SO-ZORA approach.

For the excited states and the absorption spectra, the TD-DFT approach[39] was applied to obtain the vertical excitation energies (ΔE) at the DFT/PBE ground state geometries. As density functionals, we applied the common B3LYP potential[40,41] and the range-separated hybrid functional CAMY-B3LYP[42] implemented in the ADF2013.01 code,[34] and the statistically averaged orbital potential (SAOP) showing the correct asymptotic $1/r$ behavior.[43] In order to check the sensitivity of the excited states to solvation and counterion effects, the continuum dielectric screening model COSMO was employed.[44,45] We also checked for valence-Rydberg mixing by expanding the STO basis sets of the central atoms by lower-exponent functions up to n/ζ values of about 50 ("+Ry").

CCSD(T) and CR-EOM-CCSD(T). The excited states and absorption spectral parameters as well as the vertical detachment energies of the photoelectron spectra of the MO_4^- species were determined also by SR-CCSD(T) methods, namely by the standard CC approach as implemented in the MOLPRO 2012.1 program[46] and by the CR-EOM-CC as implemented in the NWChem 6.0 program.[47] We used the Stuttgart relativistic energy-consistent pseudopotentials ECP10MDF for Mn and ECP28MDF for Tc.[48−50] Gaussian type basis sets were applied: for Mn the pseudopotential-adapted basis ECP10MDF ((8s7p6d2f1g)/[6s5p3d2f1g]),[51] for Tc the corresponding aug-cc-pVTZ basis,[50] and for O the aug-cc-pVTZ basis.[52]

The anionic ground-state geometries of MO_4^- were optimized at the SR-CCSD(T) level. Then the vertical detachment energies were determined by CCSD(T) calculations for various states of MO_4^0 at the anionic ground-state geometry. Besides, CR-EOM-CCSD(T) calculations[53] were performed as well, with the CCSD(T) energy of the third state (of $^2A_1$ symmetry) as reference. In addition, the CR-EOM-CCSD(T) method was also applied to calculate the vertical excitation energies of MO_4^- to assign the experimental absorption spectra.

The CASSCF/CCSD(T)/SO approach has been shown to yield rather accurate results in heavy-element systems.[54−60] It was used here to estimate the SO coupling effects on the photoelectron spectrum of TcO_4^-, while SO coupling is negligible for MnO_4^-. The SO coupling was included by using a state-interacting method with SO coupled relativistic pseudopotentials, whereby it is treated as a perturbation to the SR state energies. It was calculated on the basis of CASSCF wave functions with the diagonal matrix elements replaced by the individual CCSD(T) state energies. Thereby, the electron binding energies corresponding to formal one-electron transitions from the closed-shell ground state of TcO_4^- to the ground and excited states of TcO_4^0 were obtained.

RAS-PT2. For the vertical excitation energies of MO_4^- and MO_4^0 also the RAS-PT2 approach as implemented in MOLPRO 2012.1[46] was applied. The same pseudopotentials were chosen as above, while for Tc and O slightly smaller basis sets (aug-cc-pVDZ) were used and for Mn the g function in the ECP10MDF basis was removed, to save computational expenses. Diffuse functions with exponents 0.003 and 0.001 for s and 0.01 and 0.003 for p were added to allow for valence-Rydberg mixing (aug-cc-pVDZ+Ry) in test calculation for the influence of metal Rydberg orbitals.

For the MO_4^- species, the active space contained the 12 upper, doubly occupied, more or less bonding orbitals of O(2p) $1a_1$, 1e, $1t_1$, $1t_2$, and $2t_2$ character with 24 electrons, plus the 5 virtual, slightly antibonding orbitals of metal(d) 2e* and $3t_2$* character (for details, see section 3). This active space set is labeled as RAS(24e,17o). State-averaged RASSCF calculations were carried out to generate the wave functions of the ground and singlet-excited states of MO_4^-, where up to 4 electrons were allowed to be excited. In the subsequent RAS-PT2 calculations, the ionization-potential/electron-affinity corrected zeroth-order Hamiltonian[61] was used with an IPEA shift of 0.25 au. To avoid intruder states and to improve the RAS-PT2 convergence, level shifts of 0.2 and 0.3 au were applied for MnO_4^- and TcO_4^-, respectively. The excitation energies vary by less than 0.06 eV due to the level shift. Test calculations have shown that an approximate relation exists between excitation energy change Δ and level shift ls, $\Delta \approx 0.0075 \times$ ls. To test the influence of metal s- and p-type MOs, also enlarged active spaces RAS(24e,18o) with added $2a_1$ MO and RAS(24e,20o) with added $4t_2$ MOs were applied.

Similar RAS-PT2 calculations were performed on neutral TcO_4^0 with RAS(23e,17o) at the TcO_4^- ground state geometry, using IPEA shift = 0.25 au and ls = 0.2 au. RAS-PT2 calculations of MnO_4^0 however failed because of too strong configuration mixing in the MnO_4^0 states.

3. COMPUTATIONAL RESULTS AND DISCUSSION

Geometric and Electronic Structure of the Ground States of $MO_4^{0,-}$ (M = Mn, Tc). The M-O bond lengths of free MO_4^- (M = Mn, Tc) in the electronic ground-state of T_d symmetry from DFT/PBE and CCSD(T) calculations are listed in Table 1. The CCSD(T) values are 1−2 pm smaller than the DFT/PBE ones. Both are consistent with the experimental crystal data within the systematic errors of both methods.[62,63,65] Added diffuse basis functions are insignificant. The calculated totally symmetric M-O stretching vibrational frequencies ν_s(M-O) in the harmonic approximation agree within 5 and 0.2% with the experimental anharmonic values.[64]

Table 1. Ground-State Parameters of MnO_4^- and TcO_4^- (T_d Symmetry): Bond Lengths M−O (in pm) and Symmetric Breathing Vibrations ν_s (in cm^{-1}) from DFT/PBE and CCSD(T) Calculations (SR Approximation, in Vacuum), and Experimental Crystal Data

	DFT/PBE	CCSD(T)	expt, cryst
Mn−O	161.6	159.6	162.9, 161.0[62,63]
ν_s(Mn−O)	887		845[64]
Tc−O	173.55	172.5	171.1[65]
ν_s(Tc−O)	908		910[64]

dx.doi.org/10.1021/ic4009625 | Inorg. Chem. 2013, 52, 9867−9874

Remarkably, the M-O bond force constant of the heavier TcO_4^- is about 10% larger than that of MnO_4^-.

The isoelectronic TcO_4^- and MnO_4^- species have similar molecular orbital (MO) levels (Figures 1 and 3) and similar

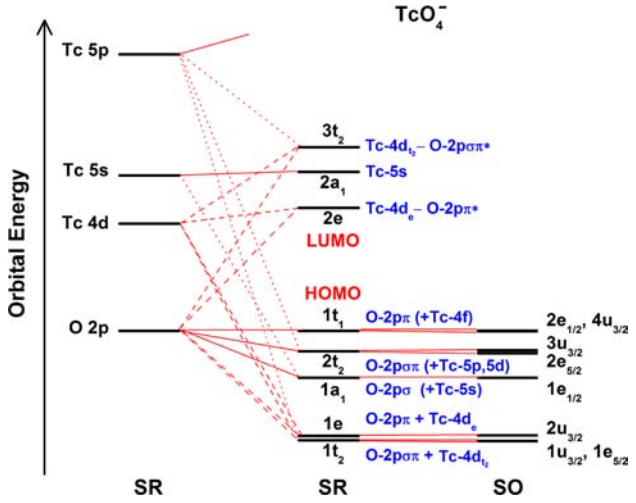

Figure 1. Qualitative valence orbital energy level scheme of Tc and O atoms at the SR level and of TcO_4^- at both the SR and SO coupling levels from DFT/PBE calculations. The connecting lines depict dominant ($>^2/_3$, solid lines), medium ($>^1/_3$, dashed lines), and weak contributions ($<^1/_{15}$, lettering in parentheses, dotted lines) of the AOs to the molecular orbitals.

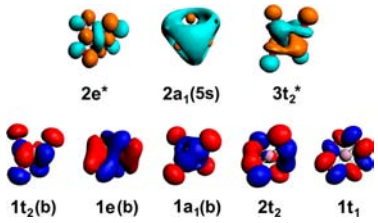

Figure 2. Valence MO contour diagrams of TcO_4^- (DFT/PBE, contour value = ± 0.03 au). $1t_2$(b) to $1t_1$ are the occupied O(2p) dominated valence MOs, 2e* to $3t_2$* are the lowest virtual MOs of Tc(4d,5s) type; (b) = bonding MO; * = antibonding MO; 5s = Rydberg MO (in this envelope diagram, its spatial extension is not visible but only the inner lobes).

orbital shapes (Figure 2). The four O(2pσ) AOs give rise to a_1 and t_2 MOs and the eight O(2pπ) AOs yield e, t_1, and t_2 MOs, with the two t_2 levels being mixed. The virtual M(d) AOs of formal M^{7+} cations stabilize the O(2p$\sigma\pi$)-$1t_2$ and O(2pπ)-1e ligand orbitals of the formal O^{2-} ligands significantly via dative bonding, and are destabilized to form antibonding 2e* and $3t_2$* orbitals. The virtual M(s) and M(p) AOs stabilize the O(2pσ)-$1a_1$ and O(2p$\sigma\pi$)-$2t_2$ orbitals slightly, whereas the highest occupied MOs (HOMOs) of O(2pπ)-$1t_1$ type remain basically nonbonding. The lowest unoccupied valence MOs (LUMOs) are of M(d)-2e*/$3t_2$* type. In neutral species one would expect molecular M(*n*s) and M(*n*p) Rydberg series, beginning with 5s and 5p in the case of Tc, and the lowest members might mix with the valence LUMOs. In the case of anions, however, there will at most be only a very few Rydberg states or even none, below the ionization limit.

The MO level schemes of the two anions are compared in Figure 3. From MnO_4^- to TcO_4^-, the main bonding levels $1t_2$

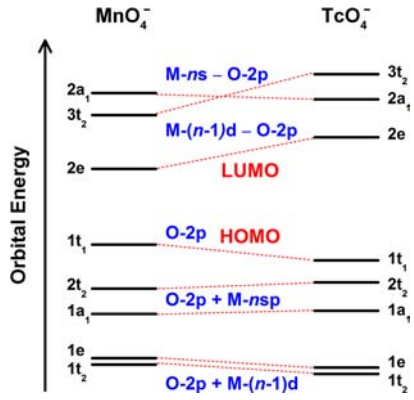

Figure 3. Comparison of occupied and virtual valence orbitals of MnO_4^- and TcO_4^- (DFT/PBE). M-*n*s is the lowest Rydberg level.

and 1e drop, corresponding to the above-mentioned increase of the stretching force constant. The bonding interaction in the heavier Tc species turns out to be stronger than in Mn, being rationalized by the more extended radial distribution of 4d versus the more compact "primogenic" 3d orbitals. Simultaneously the antibonding counterparts Tc($4d_{e^*}$) and Tc($4d_{t_2^*}$) are destabilized, leading to a modified orbital order: In TcO_4^- the only Rydberg MO level is of 5s type and lies between the $4d_{e^*}$ and $4d_{t_2^*}$ levels near the ionization limit. Due to symmetry reasons valence-Rydberg mixing does not occur.

Although the SO splitting energies of Tc are only of the order of a fraction of an eV, i.e., in the 10^3 cm^{-1} range, they are non-negligible for the spectroscopic purpose. The SO effects on the occupied MOs of TcO_4^- are indicated in Figure 1 (see also Table 3). In double-group symmetry, the a_1 and e species become $e_{1/2}$ and $u_{3/2}$ without change of degeneracy, while the t-type species are SO-split, transforming as $t_1 \rightarrow e_{1/2} \oplus u_{3/2}$, $t_2 \rightarrow e_{5/2} \oplus u_{3/2}$, respectively.

Reproduction and Prediction of Vertical Electron Detachment Energies. The calculated vertical detachment energies (VDEs) for MnO_4^- and TcO_4^- at the DFT/PBE, CCSD(T), CR-EOM-CCSD(T), and RAS-PT2 levels are displayed together with experimental and theoretical literature data in Table 2. The first three VDEs correspond to single-electron eliminations from the seven O(2p)-dominated orbitals. The nonbonding $1t_1$ and weakly bonding $2t_2$ and $1a_1$ MOs give rise to VDE values around 5, 6, and 7 eV. The two lowest strongly bonding 1e and $1t_1$ MOs yield features near 9 eV. While often the electron detachment from the bottom of the valence band is dissolved in a band of upper valence shakeup states, our correlated calculations did not show any indication of a breakdown of the orbital model.[66] In the present case, the energy distance between the first and highest valence ionization potentials is only 4 eV, and that is not sufficient for multielectronic "shakeup" excitations just a little above the first ionization.

For MnO_4^-, the calculated first VDE values from CCSD(T) and CR-EOM-CCSD(T), i.e., 4.93 and 4.91 eV, both agree well with the experimental result of 4.91 ± 0.03 eV,[67] while DFT/PBE overestimates it by nearly 0.2 eV. The present theory improves on the reported IP-EOM-CCSD result by 0.3 eV.[23] The second VDE of MnO_4^- is well reproduced by CR-EOM-

dx.doi.org/10.1021/ic4009625 | Inorg. Chem. 2013, 52, 9867−9874

Table 2. Vertical Electron Detachment Energies (VDEs in eV) of MnO_4^- and TcO_4^- in Vacuum, from DFT/PBE, CCSD(T), CR-EOM-CCSD(T) Calculations at the SR Level and from the Literature

			MnO_4^-					TcO_4^-				
			this work			ref 23	ref 67	this work				
VDE no.	MO symmetry	dominant MO character (M = Mn or Tc)	DFT/PBE[a]	CCSD(T)	CR-EOM-CCSD(T)[b]	IP-EOM-CCSD	expt	DFT/PBE[a]	CC-SD(T)	RAS-PT2	CR-EOM-CCSD(T)[b]	recommended (here)
1	$1t_1$	O2pπ(+Mf)	5.05	4.93[c]	4.91	4.59	4.9	5.33	5.59	5.61	5.07	5.3 ± 0.2
2	$2t_2$	O2pπ(+Mpd)	6.42	6.51	6.18	6.09	6.1	5.99	6.32	6.33	5.68	5.9 ± 0.2
3	$1a_1$	O2pσ(+Ms)	7.19	7.24	7.24	6.42		6.85	7.21	7.21	7.21	7.1 ± 0.2
4	1e	O2pπ(+Md)	8.37	8.61	8.86	8.95		8.73	9.16	8.88	8.82	8.8 ± 0.2
5	$1t_2$	O2pσ(+Md)	8.77	[d]	8.99	9.22		8.87	9.30	9.25	8.77	8.9 ± 0.2

[a]The third VDE corresponding to the simple $^1A_1 \rightarrow {}^2A_1$ process was calculated by the ΔSCF approach using DFT/PBE energies. The other VDEs were obtained by adding the respective orbital energy differences according to the generalized Koopmans' theorem. [b]In the CR-EOM-CCSD(T) calculations, the reference states of MnO_4 and TcO_4 have one electron detached from the $1a_1$ orbital; the reference state energies are taken from CCSD(T). [c]The CCSD(T) calculation with ECP10MDF and (8s7p6d2f1g)/[6s5p3d2f1g] basis for Mn did not converge while it converged for the same basis with the g function removed, i.e., (8s7p6d2f)/[6s5p3d2f]. The value is corrected by the [6s5p3d2f1g] − [6s5p3d2f] difference from CR-EOM-CCSD(T) calculations. [d]The CCSD(T) calculations did not converge for both the [6s5p3d2f1g] and [6s5p3d2f] basis sets.

CCSD(T) and also by IP-EOM-CCSD, while DFT/PBE and CCSD(T) overestimate it by about 0.4 eV. As for the third VDE from the $1a_1$ orbital, IP-EOM-CCSD gives 6.4 eV,[23] which is 0.8 eV less than that from CCSD(T). For the higher VDE_n (n = 4 and 5) our three methods give consistent results, which are now however lower than the IP-EOM-CCSD results by 0.1−0.4 eV. For MnO_4^-, DFT/PBE agrees reasonably well with the *ab initio* approaches within about ±0.2 eV, and CR-EOM-CCSD(T) seems most reliable both from the theoretical and the present numerical points of view.

Concerning TcO_4^-, where no experimental values are known, the VDEs from DFT/PBE, CCSD(T), and RAS-PT2 are close, with differences usually smaller than 0.37 eV, whereas the CR-EOM-CCSD(T) results are lower throughout by 0.3−0.7 eV. Concerning the changes from MnO_4^- to TcO_4^-, there is the general agreement that the VDE_n values (n = 1, 4, and 5) are larger for TcO_4^- by about 0.5 eV and VDEs 2 and 3 are somewhat smaller than for MnO_4^-. This is consistent with Koopmans' theorem and with the shift of the orbital energies as indicated in Figure 3. On this background we predict the VDEs of TcO_4^- as given in the last column of Table 2. The SO coupling effects on the VDEs of TcO_4^- from SO-DFT/PBE and CASSCF/CCSD(T)/SO calculations are listed in Table 3. VDE_5 related to the lowest bonding $1t_2$ MO is split by 0.05 eV, and VDE_2 related to the weakly bonding $2t_2$ MO by only 0.1−0.15 eV, due to mixing with Tc AOs of d- and p-type.

Reproduction and Prediction of Electronic Excitations: Absorption Spectra. Three one-electron points have to be considered (in addition to two-electron correlation) in the spectral predictions: diffuse basis orbitals, relativistic effects, and environmental perturbations.

Table 3. Spin−Orbit Effects on VDEs of TcO_4^- (in eV)

VDE no.	SR symm	SO symm	CC-SD(T)	CCSD(T) SI/SO	DFT/PBE SR-ZORA	DFT/PBE SO-ZORA
1a	$1t_1$	$4u_{3/2}$	5.59	5.59	5.33	5.33
1b		$2e_{1/2}$		5.59		5.34
2a	$2t_2$	$3u_{3/2}$	6.32	6.27	5.99	5.96
2b		$2e_{5/2}$		6.42		6.06
3	$1a_1$	$1e_{1/2}$	7.21	7.21	6.85	6.85
4	1e	$2u_{3/2}$	9.16	9.15	8.73	8.72
5a	$1t_2$	$1e_{5/2}$	9.30	9.27	8.87	8.84
5b		$1u_{3/2}$		9.32		8.90

MnO_4^-. The UV−vis absorption spectrum of MnO_4^- has become the paradigm for ligand-to-metal charge-transfer (LMCT) in transition-metal spectroscopy. The MnO_4^- ion is one of the benchmark systems for assessing the performance of quantum chemical methods for excited states. Such closed-shell complexes are more complex than it might seem, and much theoretical effort has already been invested, e.g., in refs 21 and 28. In T_d symmetry the spin- and dipole-allowed transitions of MnO_4^- are from the $^1A_1$ ground state to $^1T_2$ excited states. We have performed TDDFT/SAOP, CR-EOM-CCSD(T), and RAS-PT2 calculations with standard polarized-diffused basis sets and with added Rydberg functions (+Ry), in vacuum and in a continuum dielectric solvent model (COSMO). The results are compared with vacuum SAC-CI calculations[21] and with experimental data for the crystals[15] in Table 4.

For excitation energies up to 1−2 eV above the ionization limit, the addition of extended basis sets is of minor influence. Also, the COSMO[44,45] calculations simulating solvent embedding showed little change. Obviously, the Rydberg orbitals in MnO_4^- are too high in energy to have an influence on the lower valence spectra. Upon the valence excitations, the rather symmetric ligand to metal charge transfer "inside" the molecule is hardly affected by a continuous solvent. This might be different if hydrogen bonding by water molecules would be treated explicitly. Spin−orbit couplings in Mn are smaller than the present reliability of the calculations and were not accounted for.

As mentioned above, the occupied valence shell of MO_4^- comprises 7 nearly nonbonding (nb) O-lonepair orbitals of $1t_1$, $2t_2$, and $1a_1$ type, and 5 $O(2p_{\sigma,\pi}) \rightarrow$ M dative bonding (b) orbitals of 1e and $1t_2$ type. The 5 lowest virtual orbitals are antibonding (*) and of d-2e and d-$3t_2$ type. The expected 4 lowest Rydberg orbitals of Mn(4s)-$2a_1$ and Mn(4p)-$4t_2$ type turn out to be significantly higher in energy. One expects up to 8 spin- and dipole-allowed LMCT $^1A_1 \rightarrow {}^1T_2$ excitations, 5 ones of nb → * type and 3 ones of b → * type, several of them below the ionization threshold. They will exhibit vibronic Jahn−Teller progressions, and several ones are known to be strongly configuration mixed.[28]

There are four observed and calculated allowed transitions in the energy range up to about 6 eV. The excited terms 1^1T_2 to

dx.doi.org/10.1021/ic4009625 | Inorg. Chem. 2013, 52, 9867−9874

Table 4. Vertical Singlet Excitations of MnO_4^-[a]

term	main config	TDDFT SAOP ΔE ($10^3 f$)	TDDFT SAOP +Ry ΔE ($10^3 f$)	SAOP +COSMO +Ry ΔE ($10^3 f$)	RAS-PT2 ΔE ($10^3 f$)	CR-EOM-CCSD(T): ΔE	SAC- CI[21] ΔE ($10^3 f$)	expt[15] ΔE (I)
X^1A_1		0	0	0	0	0	0	0
1^1T_1	$1t_1 \rightarrow 2e$	2.66	2.65	2.65	1.93	2.00	2.18	
1^1T_2	$1t_1 \rightarrow 2e$	3.08(7.4)	3.06(7.6)	3.07(7.5) [+0.7]	2.33(4.2) [−0.1]	2.50 [+0.1]	2.57(2.0) [+0.2]	2.4(S)
2^1T_1	$2t_2 \rightarrow 2e$	3.91	3.90	3.91	3.39	3.49	3.33	
2^1T_2	$1t_1 \rightarrow 3t_2$, $2t_2 \rightarrow 2e$	4.12(2.0)	4.11(2.4)	4.12(2.4) [+0.5]	3.53(1.5) [−0.1]	3.83 [+0.2]	3.58(4.5) [−0.0]	3.6(m)
1^1E	$1t_1 \rightarrow 3t_2$	4.50	4.48	4.49	3.90	3.80	3.41	
2^1E	$1a_1 \rightarrow 2e$	4.70	4.71	4.70	4.23	3.97	3.54	
3^1T_1	$1t_1 \rightarrow 3t_2$	4.44	4.42	4.43	3.93	4.10	4.12	
3^1T_2	$2t_2 \rightarrow 2e$, $1t_1 \rightarrow 3t_2$	5.01(9.1)	4.97(10)	4.99(10) [+0.9]	4.20(6.1) [+0.1] 4.53(0.0)	4.03 [−0.1]	3.72(14) [−0.4]	4.1(S)
1^1A_2	$1t_1 \rightarrow 3t_2$	4.31	4.29	4.31	3.89	4.13	4.46	
				Ionization Limit				
4^1T_1	$2t_2 \rightarrow 3t_2$	5.72	5.69	5.71	5.21	5.19[c]	5.30	
2^1A_1	$2t_2 \rightarrow 3t_2$	5.75	5.73	5.75	5.10	5.39	5.41	
3^1E	$2t_2 \rightarrow 3t_2$	5.66	5.64	5.66	5.22	5.46	5.47	
2^1A_2	$1e \rightarrow 2e$	5.92	5.91	5.91	5.09	5.84		
4^1T_2	$1a_1 \rightarrow 3t_2$, $2t_2 \rightarrow 3t_2$, $1t_2 \rightarrow 2e$	6.08(3.1)	6.06(5.1)	6.07(4.3) [+0.6]	5.62(0.0) 5.72(1.7) [+0.2]	5.84 [+0.3]	5.82(2.2) [+0.3]	~5.5(m)

[a]Vertical excitation energies ΔE (in eV, deviation from experimental values in square brackets); and oscillator strength f or relative intensities I (in parentheses in the same line; S = strong, m = medium, w = weak), from present TDDFT/SAOP, RAS(24e,17o)-PT2, and CR-EOM-CCSD(T) calculations (in vacuum, or in continuum solvent = +COSMO; with standard basis or with added Rydberg basis = +Ry) and comparison with SAC-CI and experimental values from the literature.

4^1T_2 correspond to mixtures of singly substituted ground-state configurations of nb → * character. Our RAS-PT2 and CR-EOM-CCSD(T) energies and the SAC-CI values in the literature deviate from the observed ones by ±0.2 eV The TDDFT/SAOP results deviate more, by +0.7 ± 0.2 eV. The calculated oscillator strengths are qualitatively reasonable. Within an error range of ±0.3 eV, also the dipole-forbidden excitations have a consistent order in the four theoretical methods.

TcO_4^-. Well-resolved UV absorption spectra of TcO_4^- in crystals at He temperature were reported by Güdel and Ballhausen in 1972.[7] The experimental spectra display two strong overlapping bands with distinct vibrational structures, at maxima around 4.35 and 5.1 eV. A low-resolved electronic spectrum of TcO_4^- in the vapor phase showed a weak band at 6.6 eV in addition.[6] The electronic excitations in TcO_4^- are similar to those in MnO_4^-, yet the former have been less intensively investigated by theory. Nakatsuji et al.[11] determined the 17 lowest excitations in the energy range up to 8.25 eV using the SAC-CI approach and reproduced the three observed transition energies within 0.4 eV. Stückl et al.[9] also reproduced them within an error range of 0.4 eV using the DFT transition state approximation. Ziegler et al.[10] determined only the first two $^1T_2$ terms with TDDFT/LDA, within 0.25 eV.

We have calculated the electronic states of TcO_4^- with the TDDFT (with B3LYP, CAMY-B3LYP, and SAOP functionals), and the CR-EOM-CCSD(T) and RAS(24e,17o or 18o or 20o)-PT2 approaches. Some of our results for the lowest terms up to about 7 eV are listed in Table 5 and compared with the reported SAC-CI[11] and experimental data.[6,7] The energies from the different density functionals (including the range separated CAMY and asymptotically correct SAOP ones, see the CAMY-B3LYP results in the Supporting Information file) scatter within ±0.1 eV. Compared with the WFT results, the DFT excitation energies tend to be 0.5 eV higher. The different WFT energies also agree within about ±0.15 eV, except that the higher excitations from the SAC-CI approach in the literature tend to be higher than our present WFT results. The addition of diffuse Rydberg basis functions has a negligible influence on the excitation energies of O(2p) → Tc(4d) character, in particular for solvent-embedded TcO_4^-. The oscillator strengths vary between the methods by some 1-digit factors and show rough qualitative agreement with each other and with the qualitatively observed intensities.

Remarkably, when Rydberg basis functions are included in the basis, a few excited states of Rydberg type of the isolated TcO_4^- ion in vacuum appear in WFT calculations above the ionization limit. The O(2p) → Tc(5s Rydberg) excitations are interlaced between the O(2p) → Tc($4d_{e^*}$) and O(2p) → Tc($4d_{t_2^*}$) excitations. The diffuse outer parts of the wave functions are weakly coupled to the inner-molecular valence MO tails, leading to weak oscillator strengths. The excited Rydberg type states of TcO_4^- ion in vacuum disappeared in the solvent model. That is, they will not show up in condensed phase spectra and will hardly be visible in vacuum spectra. Therefore, we performed most of the more accurate calculations using standard extended basis sets and no solvent embedding. The results should be comparable to real experimental spectra. The two observed energies in the middle UV region agree with the calculated ones of O(2p,nb) → Tc($4d_{e^*}$) type within ±0.2 eV. The qualitative intensity ratio agrees too. The observed weak band more than 1 eV above the ionization limit may be due to excitations of local O(2p,nb) → Tc($4d_{t_2^*}$) type. The agreements give confidence in the other excited state energies within about ±0.2 eV.

Comparison of MnO_4^- and TcO_4^-. The lower dipole-excitable $^1T_2$ states of the two anions are compared in Table 6 at the RAS configuration-mixing perturbation-theory corrected level. All states are heavily configuration-mixed (compare, e.g., refs 28 and 68). The RAS-PT2 approach gives good agreement concerning the energies and intensities of both anions. The first

dx.doi.org/10.1021/ic4009625 | Inorg. Chem. 2013, 52, 9867−9874

Table 5. Vertical Singlet Excitations of TcO_4^-[a]

term	main config	TDDFT SAOP ΔE (10^3f)	TDDFT B3LYP ΔE (10^3f)	B3LYP +COSMO +Ry ΔE (10^3f)	CR-EOM CCSD(T): ΔE	RAS-PT2 +Ry ΔE (10^3f)	SAC-CI[11] ΔE (10^3f)	expt[7] ΔE (I)
X^1A_1		0	0	0	0	0	0	0
1^1T_1	$1t_1 \rightarrow 2e$	4.25	4.06	4.05	3.74	3.84	3.83	
1^1T_2	$1t_1 \rightarrow 2e, 2t_2 \rightarrow 2e$	4.59(7.8) [+0.2]	4.48 [+0.1]	4.48 [+0.1]	4.12 [−0.2]	4.19(4.7) [−0.15]	4.28(17.) [−0.1]	4.35(m)
2^1T_1	$2t_2 \rightarrow 2e$	4.83	4.78	4.77	4.54	4.66	4.61	
2^1T_2	$1t_1 \rightarrow 2e, 2t_2 \rightarrow 2e, 1t_1 \rightarrow 3t_2$	5.30(20.) [+0.2]	5.32 [+0.2]	5.30 [+0.2]	5.07 [+0.0]	5.08(9.3) [0.0]	5.29(42.) [+0.2]	5.1(S)
1^1E	$1a_1 \rightarrow 2e$	5.68	5.65	5.64	5.32	5.29	4.98	
				Ionization Limit				
3^1T_1	$1t_1 \rightarrow 3t_2, 1t_1 \rightarrow 2a_1Ry$	6.28	6.22, 6.20	6.21	5.70	5.53	6.42	
2^1E	$1t_1 \rightarrow 3t_2$	6.38	6.20	6.18	5.83	6.01	6.08	
3^1T_2	$1t_1 \rightarrow 3t_2, 2t_2 \rightarrow 3t_2$	6.61(3.8) [0.0]	6.41 [−0.2]	6.36 [−0.25]	5.90 [−0.7]	6.07	6.20(2.5) [−0.4]	6.6(w)
1^1A_2	$1t_1 \rightarrow 3t_2$	6.18	6.14	6.13	5.94	6.04	6.54	
4^1T_1	$2t_2 \rightarrow 3t_2, 1t_1 \rightarrow 3t_2, 1t_1 \rightarrow 2a_1Ry$	6.87	6.89	6.86, 6.78	5.94	6.05	6.95	
3^1E	$2t_2 \rightarrow 3t_2, 1t_1 \rightarrow 3t_2$	6.83	6.89	6.86	6.13	6.79	7.19	

[a]Vertical excitation energies ΔE (in eV, deviation from experimental values in square brackets); and oscillator strength f or relative intensities I (in parentheses in the same line; S = strong, m = medium, w = weak), from present TDDFT/SAOP, TDDFT/B3LYP, RAS(24e,18o)-PT2, and CR-EOM-CCSD(T) calculations (in vacuum, or in continuum solvent = +COSMO; with standard basis or with added Rydberg basis = +Ry) and comparison with SAC-CI and experimental values from the literature. In column 2, Ry means molecular levels of Rydberg character.

three observed (and calculated) singlet-excitations of TcO_4^- are about 2 eV higher than those of MnO_4^-, corresponding to the stronger bonding occupied MOs and the stronger antibonding virtual MOs of the former, heavier species (see Figure 3). Only the first 3 excitations of MnO_4^- and the first 2 ones of TcO_4^- are below the ionization limit. For MnO_4^- the calculated fourth and fifth $^1T_2$ terms with very small predicted oscillator strengths have not been observed, but the sixth one with sufficiently high transition probability. In reality, it is a broad resonance in the continuum, of inner molecular localized type, and no Rydberg admixture is to be expected, in particular not in the crystal. The configuration mixing and transition dipoles of the $^1T_2$ terms of TcO_4^- differ from those of MnO_4^-, yielding different spectral shapes. Namely, the third and fourth excitations of the Tc species just above the ionization limit have comparable medium intensities, giving rise to a broad overlapped band, while the next two transitions are not expected to be observable in the continuum due to their high energies and low transition moments.

4. SUMMARY AND CONCLUSIONS

Electronic excitations and detachments of MnO_4^- and TcO_4^- have been calculated, applying DFT, CC, and RAS-PT2 approaches. The comparison with the available experimental data for TcO_4^- and MnO_4^- gives us confidence in our predictions of the ionizations and excitations of TcO_4^-. The three highest MO levels of $1a_1$, $2t_2$, and $1t_1$ symmetry are of basically nonbonding O(2p$\sigma\pi$) type and will give detachment energies below 7.5 eV (around 5.3, 5.9, and 7.1 eV, respectively). The lower two MO levels of 1e and $1t_2$ symmetry are of Tc(4d) ← O(2p) bonding type and will give electronically and vibrationally broadened detachment features around 9 eV. We did not find any indication of a "breakdown of the orbital picture" at the bottom of the O(2p)−M(d) valence band. The largest spin−orbit energy splitting of the heavier species occurs for the $2t_2$ O(2p) MO, due to Tc(5p) valence shell admixture. It is still as small as 0.15 eV, corresponding to the 5% admixture of Tc-4p-core orbitals. Concerning MnO_4^-, where two experimental detachment energies are available, the presently applied CR-EOM-CCSD(T) approach leads to an (expected) improvement over the IP-EOM-CCSD(T) one.[23]

As mentioned, both "closed shell" complexes have heavily configuration-mixed ground and excited states, and the electronic ligand-to-metal charge transfer excitations are far from single-electron excitation type. Therefore, TDDFT without proper correction of the self-interaction error (SIE) is not recommendable for the electronic excitations of such complexes, although one obtains reasonably small deviations for TcO_4^-, probably due to fortuitous error cancellation. The observed absorption peaks in the electronic spectra of MnO_4^- and TcO_4^- (four and three peaks, respectively) are assigned to dipole-allowed $^1A_1 \rightarrow {}^1T_2$ (nb → *) transitions on the basis of RAS-PT2 calculations. The fourth and fifth $^1T_2$ excitations of MnO_4^- have not yet been observed owing to their low calculated intensities. The observed fourth broad strong feature correlates well with the sixth $^1A_1 \rightarrow 6^1T_2$ transition of RAS-PT2. Remarkably, refs 21, 22, 26, 27 had assigned the strong fourth absorption to the fourth or fifth $^1T_2$ term, despite the low expected intensities for $^1A_1 \rightarrow 4,5^1T_2$. The observed highest absorption features of MnO_4^- and TcO_4^- are already in the continuum, and much more structure will hardly be observable. Due to the negative charge of the species under discussion, the influence of Rydberg states is minor. In the case

dx.doi.org/10.1021/ic4009625 | Inorg. Chem. 2013, 52, 9867−9874

Table 6. Dipole-Allowed $^1A_1 \rightarrow {}^1T_2$ Excitations of MnO_4^- and TcO_4^- in Condensed Phase, RAS-PT2, and UV-Spectroscopic Results[a]

	MnO_4^-			TcO_4^-		
term 1	main configs	ΔE ($10^3 f$)	ΔE_{exp} (I)	main configs	ΔE ($10^3 f$)	ΔE_{exp} (I)
$^1T_2$	$1t_1 \rightarrow 2e$, $2t_2 \rightarrow 2e$	2.33 (4.2)	2.4 (S)	$1t_1 \rightarrow 2e$, $2t_2 \rightarrow 2e$	4.19 (4.7)	4.3 (m)
2^1T_2	$2t_2 \rightarrow 2e$, $1t_1 \rightarrow 3t_2$	3.53 (1.5)	3.6 (m)	$1t_1 \rightarrow 2e$, $2t_2 \rightarrow 2e$	5.08 (9.3)	5.1 (S)
3^1T_2	$1t_1 \rightarrow 3t_2$, $2t_2 \rightarrow 2e$, $2t_2 \rightarrow 3t_2$, $1t_1 \rightarrow 2e$	4.20 (6.1)	4.1 (S)	$1t_1 \rightarrow 3t_2$, $2t_2 \rightarrow 3t_2$	6.07 (4.3)	6.6 (w)
4^1T_2	$1t_1 \rightarrow 3t_2$, $2t_2 \rightarrow 2e$	4.53 (0.0)	n.o.	$2t_2 \rightarrow 3t_2$, $1t_2 \rightarrow 2e$, $1a_1 \rightarrow 3t_2$	7.33 (3.0)	
5^1T_2	$1a_1 \rightarrow 3t_2$, $2t_2 \rightarrow 3t_2$	5.62 (0.0)	n.o.			
6^1T_2	$1t_2 \rightarrow 2e$, $1a_1 \rightarrow 3t_2$	5.72 (1.7)	5.5 (m)			

[a]At CCSD(T) ground-state geometry: Mn−O = 160.29 pm, Tc−O = 173.76 pm; ΔE is the vertical excitation energy in eV (in parentheses; f is the oscillator strength, I the qualitative intensity; S = strong, m = medium, w = weak). Main configs = leading singly substituted configuration(s). The ionization limit is indicated by a heavy line.

of Mn, the Rydberg states are shifted too high into the continuum. In the case of Tc, the lowest 5s Rydberg level is near zero-energy above the bound Tc($4d_{e^*}$) level and below the Tc($4d_{e^*}$) continuum-resonance level. However, in the crystal or in solution the Rydberg admixture to molecule-localized valence-excited states is suppressed.

We have presented the first study of the excited states of MnO_4^- and TcO_4^- using the CR-EOM-CCSD(T) and RASPT2 methods. Our results show that both dynamic and nondynamic electron correlations are very important in the ground and excited states of MnO_4^- and TcO_4^-. Especially, the nondynamic electron correlation of MnO_4^- can already be well recovered at the quadruple substitution level based on our RASSCF calculations. Remarkably, larger active spaces and higher electronic substitutions are needed for reliable excitation energy predictions of the heavier homologue TcO_4^-, which is also bound more strongly.

■ ASSOCIATED CONTENT

Ⓢ Supporting Information

Calculated vertical singlet excitations (energies and oscillator strengths) of MnO_4^- and TcO_4^- from TDDFT (with SAOP, CAMY-B3LYP, and B3LYP functionals) and RAS-PT2 methods. This material is available free of charge via the Internet at http://pubs.acs.org.

■ AUTHOR INFORMATION

Corresponding Author

*E-mail: junli@mail.tsinghua.edu.cn.

Present Address

[§]Physical and Theoretical Chemistry, University of Siegen, Am Brünkel 24, Siegen 57074, Germany. E-mail: schwarz@chemie.uni-siegen.de.

Notes

The authors declare no competing financial interest.

■ ACKNOWLEDGMENTS

We acknowledge the financial support by NSFC (11079006, 91026003) to J.L. and NSFC (21201106) and the China Postdoctoral Science Foundation (2012M520297) to J.S. The calculations were performed at the Supercomputer Center of the Computer Network Information Center, Chinese Academy of Sciences, the Shanghai Supercomputing Center, and the Tsinghua National Laboratory for Information Science. A portion of the calculations was performed using EMSL, a national scientific user facility sponsored by the US-DOE's Office of Biological and Environmental Research and located at the Pacific Northwest National Laboratory.

■ REFERENCES

(1) Schwochau, K. *Technetium: Chemistry and Radiopharmaceutical Applications*; Wiley-VCH: Weinheim, 2000.
(2) Schwochau, K. *Angew. Chem., Int. Ed.* **1994**, *33*, 2258.
(3) IAEA. *Technetium-99m Radiopharmaceuticals: Status and Trends*; International Atomic Energy Agency: Vienna, 2009.
(4) Dileep, C. S.; Jagasia, P.; Dhami, P. S.; Achuthan, P. V.; Dakshinamoorthy, A.; Tomar, B. S.; Munshi, S. K.; Dey, P. K. *Desalination* **2008**, *232*, 157.
(5) Kumari, N.; Pathak, P. N.; Prabhu, D. R.; Manchanda, V. K. *Sep. Sci. Technol.* **2011**, *46*, 79.
(6) Mullen, P.; Schwochau, K.; Jørgensen, C. K. *Chem. Phys. Lett.* **1969**, *3*, 49.
(7) Güdel, H. U.; Ballhausen, C. J. *Theor. Chim. Acta* **1972**, *25*, 331.
(8) Ziegler, T.; Rauk, A.; Baerends, E. *J. Chem. Phys.* **1976**, *16*, 209.
(9) Stückl, A. C.; Daul, C. A.; Güdel, H. U. *J. Chem. Phys.* **1997**, *107*, 4606.
(10) Jose, L.; Seth, M.; Ziegler, T. *J. Phys. Chem. A* **2012**, *116*, 1864.
(11) Hasegawa, J.; Toyota, K.; Hada, M.; Nakai, H.; Nakatsuji, H. *Theor. Chim. Acta* **1995**, *92*, 351.
(12) Su, J.; Wei, F.; Schwarz, W. H. E.; Li, J. *J. Phys. Chem. A* **2012**, *116*, 12299.
(13) Teltow, J. *Z. Phys. Chem. B* **1938**, *40*, 397.
(14) Teltow, J. *Z. Phys. Chem. B* **1939**, *43*, 198.
(15) Holt, S. L.; Ballhausen, C. J. *Theor. Chim. Acta* **1967**, *7*, 313.
(16) Hillier, I. H.; Saunders, V. R. *Proc. R. Soc. London, Ser. A* **1970**, *320*, 161.
(17) Hillier, I. H.; Saunders, V. R. *Chem. Phys. Lett.* **1971**, *9*, 219.
(18) Hsu, H.-l.; Peterson, C.; Pitzer, R. M. *J. Chem. Phys.* **1976**, *64*, 791.
(19) Johansen, H.; Rettrup, S. *Chem. Phys.* **1983**, *74*, 77.
(20) Johansen, H. *Mol. Phys.* **1983**, *49*, 1209.
(21) Nakai, H.; Ohmori, Y.; Nakatsuji, H. *J. Chem. Phys.* **1991**, *95*, 8287.
(22) Nooijen, M. *J. Chem. Phys.* **1999**, *111*, 10815.
(23) Nooijen, M.; Lotrich, V. *J. Chem. Phys.* **2000**, *113*, 494.
(24) Johnson, K. H.; Smith, F. C., Jr. *Chem. Phys. Lett.* **1971**, *10*, 219.
(25) Stückl, A. C.; Daul, C. A.; Güdel, H. U. *J. Chem. Phys.* **1997**, *107*, 4606.
(26) van Gisbergen, S. J. A.; Snijders, J. G.; Baerends, E. J. *Comput. Phys. Commun.* **1999**, *118*, 119.
(27) Boulet, P.; Chermette, H.; Daul, C.; Gilardoni, F.; Rogemond, F.; Weber, J.; Zuber, G. *J. Phys. Chem. A* **2001**, *105*, 885.
(28) Neugebauer, J.; Baerends, E. J.; Nooijen, M. *J. Phys. Chem. A* **2005**, *109*, 1168.
(29) Vancoillie, S.; Zhao, H.; Tran, V. T.; Hendrickx, M. F. A.; Pierloot, K. *J. Chem. Theory Comput.* **2011**, *7*, 3961.
(30) Wei, F.; Wu, G. S.; Schwarz, W. H. E.; Li, J. *J. Chem. Theory Comput.* **2011**, *7*, 3223.

(31) Wei, F.; Wu, G. S.; Schwarz, W. H. E.; Li, J. *Theor. Chem. Acc.* **2011**, *129*, 467.
(32) Su, J.; Schwarz, W. H. E.; Li, J. *Inorg. Chem.* **2012**, *51*, 3231.
(33) Perdew, J. P.; Burke, K.; Ernzerhof, M. *Phys. Rev. Lett.* **1996**, *77*, 3865.
(34) See http://www.scm.com for ADF 2010.02 and ADF 2013.01, SCM, Theoretical Chemistry, Vrije Universiteit, Amsterdam, The Netherlands.
(35) Fonseca Guerra, C. F.; Snijders, J. G.; te Velde, G.; Baerends, E. J. *Theor. Chem. Acc.* **1998**, *99*, 391.
(36) te Velde, G.; Bickelhaupt, F. M.; Baerends, E. J.; Guerra, C. F.; van Gisbergen, S. J. A.; Snijders, J. G.; Ziegler, T. *J. Comput. Chem.* **2001**, *22*, 931.
(37) van Lenthe, E.; Baerends, E. J.; Snijders, J. G. *J. Chem. Phys.* **1993**, *99*, 4597.
(38) van Lenthe, E.; Baerends, E. J. *J. Comput. Chem.* **2003**, *24*, 1142.
(39) van Gisbergen, S. J. A.; Snijders, J. G.; Baerends, E. J. *Comput. Phys. Commun.* **1999**, *118*, 119.
(40) Becke, A. D. *Phys. Rev. A* **1988**, *38*, 3098.
(41) Lee, C.; Yang, W.; Parr, R. G. *Phys. Rev. B* **1988**, *37*, 785.
(42) Seth, M.; Ziegler, T. *J. Chem. Theory Comput.* **2012**, *8*, 901.
(43) Schipper, P. R. T.; Gritsenko, O. V.; van Gisbergen, S. J. A.; Baerends, E. J. *J. Chem. Phys.* **2000**, *112*, 1344.
(44) Klamt, A.; Schüürmann, G. *J. Chem. Soc., Perkin Trans.* **1993**, *2*, 799.
(45) Pye, C. C.; Ziegler, T. *Theor. Chem. Acc.* **1999**, *101*, 396.
(46) Werner, H. J.; Knowles, P. J.; Knizia, G.; Manby, F. R.; Schütz, M.; et al. *MOLPRO, Version 2012.1, A Package of ab Initio Programs*; see http://www.molpro.net.
(47) Valiev, M.; Bylaska, E. J.; Govind, N.; Kowalski, K.; Straatsma, T. P.; Van Dam, H. J. J.; Wang, D.; Nieplocha, J.; Apra, E.; Windus, T. L.; de Jong, W. *Comput. Phys. Commun.* **2010**, *181*, 1477.
(48) Dolg, M. http://www.tc.uni-koeln.de/PP/clickpse.en.html.
(49) Dolg, M.; Wedig, U.; Stoll, H.; Preuss, H. *J. Chem. Phys.* **1987**, *86*, 866.
(50) Peterson, K. A.; Figgen, D.; Dolg, M.; Stoll, H. *J. Chem. Phys.* **2007**, *126*, 124101.
(51) Martin, J. M. L.; Sundermann, A. *J. Chem. Phys.* **2001**, *114*, 3408.
(52) Kendall, R. A.; Dunning, T. H.; Harrison, R. J. *J. Chem. Phys.* **1992**, *96*, 6796.
(53) Kowalski, K.; Piecuch, P. *J. Chem. Phys.* **2004**, *120*, 1715.
(54) Wang, X. B.; Wang, Y. L.; Yang, J.; Xing, X. P.; Li, J.; Wang, L. S. *J. Am. Chem. Soc.* **2009**, *131*, 16368.
(55) Wang, Y. L.; Zhai, H. J.; Xu, L.; Li, J.; Wang, L. S. *J. Phys. Chem. A* **2010**, *114*, 1247.
(56) Wang, Y. L.; Wang, X. B.; Xing, X. P.; Wei, F.; Li, J.; Wang, L. S. *J. Phys. Chem. A* **2010**, *114*, 11244.
(57) Liu, H. T.; Xiong, X. G.; Dau, P. D.; Wang, Y. L.; Li, J.; Wang, L. S. *Chem. Sci.* **2011**, *2*, 2101.
(58) Su, J.; Wang, Y. L.; Wei, F.; Schwarz, W. H. E.; Li, J. *J. Chem. Theory Comput.* **2011**, *7*, 3293.
(59) Dau, P. D.; Su, J.; Liu, H. T.; Liu, J. B.; Huang, D. L.; Li, J.; Wang, L. S. *Chem. Sci.* **2012**, *3*, 1137.
(60) Dau, P. D.; Su, J.; Liu, H. T.; Huang, D. L.; Li, J.; Wang, L. S. *J. Chem. Phys.* **2012**, *137*, 064315.
(61) Ghigo, G.; Roos, B. O.; Malmqvist, P. Å. *Chem. Phys. Lett.* **2004**, *396*, 142.
(62) Palenik, G. J. *Inorg. Chem.* **1967**, *6*, 503.
(63) Boonstra, E. G. *Acta Crystallogr., Sect. B* **1968**, *24*, 1053.
(64) Müller, A.; Baran, E. J.; Carter, R. O. *Struct. Bonding (Berlin)* **1976**, *26*, 81.
(65) Krebs, B.; Hasse, K.-D. *Acta Crystallogr., Sect. B* **1976**, *32*, 1334.
(66) Cederbaum, L S; Schirmer, J.; Domcke, W.; von Niessen, W. *Adv. Chem. Phys.* **1986**, *65*, 115.
(67) Gutsev, G. L.; Rao, B. K.; Jena, P.; Wang, X. B.; Wang, L. S. *Chem. Phys. Lett.* **1999**, *312*, 598.
(68) Buijse, M. A.; Baerends, E. J. *J. Chem. Phys.* **1990**, *93*, 4129.